Chapter 7 Feasibility study of alloy $Al_{80}Mg_{20}$% weight, heat-treated as energy material

Capítulo 7 Estudio de la factibilidad de la aleación $Al_{80}Mg_{20}$%peso, tratado térmicamente como material energético

REDA-CRUZ, Alfredo†, PÉREZ-MONTEJO, Salatiel, CALAN-CANCHE, Damian and FLORES-CHAN, José Enrique*

Universidad Autónoma del Carmen, Campus III, Facultad de Ingeniería, Avenida Central S/N, Esq. Con Fracc. Mundo Maya, C.P. 24115, Ciudad del Carmen, Campeche, México.

ID 1st Author: *Alfredo, Reda-Cruz* / **ORC ID:** 0000-0002-8767-3616, **CVU CONAHCYT ID:** 952544

ID 1st Co-author: *Salatiel, Pérez-Montejo* / **ORC ID:** 0000-0002-1750-0154, **CVU CONAHCYT ID:** 594590

ID 2nd Co-author*: José Damian, Calan-Canche* / **ORC ID:** 0000-0001-6688-4468, **CVU CONAHCYT ID:** 415663

ID 3rd Co-author: *José Enrique, Flores-Chan* / **ORC ID:** 0000-0003-4714-686X, **CVU CONAHCYT ID:** 175430

DOI: 10.35429/H.2023.6.67.75

*Jeflores@pampano.unacar.mx

S. Vargas, S. Figueroa, C. Patiño and J. Sierra (AA. VV.) Engineering and Applied Sciences. Handbooks-TI-©ECORFAN-Mexico, Mexico City, 2023

Abstract

The purpose of this research is to evaluate the effect of the aging heat treatment and the electrochemical behavior of the alloy ($Al_{80}Mg_{20}$% weight), for energy purposes through corrosion processes. Hydrogen generation sources currently have a high cost, and their large-scale implementation has been of great interest in research. Aluminum and its alloys have great potential as energetic materials due to their low cost, performance, and availability. The Aluminum-Magnesium alloy $Al_{80}Mg_{20}$% weight was obtained by casting and subsequently subjected to an aging heat treatment that favored microstructural heterogeneity and the precipitation of the β intermetallic phase (Al_3Mg_2). This $Al_{80}Mg_{20}$% weight alloy was characterized by optical microscopy, scanning electron microscopy and X-ray diffraction. The electrochemical behavior of the $Al_{80}Mg_{20}$% weight alloy was also characterized by Open Circuit Potential (PCA), Potentiodynamic Polarization Curves (CPP) and Electrochemical Impedance Spectroscopy (EIE). The results indicated a change in the microstructural morphology of the polygonal type and the presence of cracks at the grain boundaries, as well as the presence of the α Al (Mg) phase and a β (Al_3Mg_2) intermetallic secondary phase, with a higher precipitation in the grain boundaries, both with a cubic crystallographic system. Through the PCA, corrosion current density (Icorr), anodic and cathodic Tafel slopes (β and α). They showed that both samples are susceptible to embrittlement corrosion, with the rate of corrosion being more accentuated in the sample after $Al_{80}Mg_{20}$-6TT350°C.

Corrosion, Intermetallic, Cracking, Embrittlement

Resumen

El propósito de esta investigación es evaluar el efecto del tratamiento térmico de envejecido y el comportamiento electroquímico de la aleación ($Al_{80}Mg_{20}$% peso), para fines energéticos mediante procesos de corrosión. Las fuentes de generación de hidrógeno en la actualidad tienen un alto costo y su implementación a gran escala ha sido de gran interés. El aluminio y sus aleaciones tienen mucho potencial como materiales energéticos por el bajo costo, el rendimiento y disponibilidad. La aleación de Aluminio-Magnesio ($Al_{80}Mg_{20}$% peso), se obtuvo por fundición y posteriormente se le practicó un tratamiento térmico de envejecido que favoreció la heterogeneidad microestructural y la precipitación de la fase intermetálica β (Al_3Mg_2). La aleación $Al_{80}Mg_{20}$%peso, se caracterizó por Microscopía óptica, Microscopia electrónica de barrido y Difracción de rayos X. También se caracterizó el comportamiento electroquímico de la aleación $Al_{80}Mg_{20}$% peso mediante Potencial a circuito abierto (PCA), Curvas de polarización potenciodinámica (CPP) y Espectroscopia de Impedancia Electroquímica (EIE). Los resultados indicaron un cambio en la morfología microestructural del tipo poligonal y presencia de agrietamientos en los límites de grano, así como la presencia de la fase α Al (Mg) y una fase secundaria intermetálica β(Al_3Mg_2), con una mayor precipitación en los límites de grano, ambas con un sistema cristalográfico cubico. A través del PCA, densidad de corriente de corrosión (Icorr) y pendientes anódica y catódica de Tafel (β y α), revelaron que ambas muestras son susceptibles a la corrosión por fragilización, siendo más acentuada la velocidad de corrosión en la muestra $Al_{80}Mg_{20}$-6TT350°C.

Corrosión, Intermetálico, Agrietamientos, Fragilización

1. Introduction

Aluminum alloys of the 5xxx series, have Mg as the main alloying element, its maximum solubility in Al is 17.4% and its precipitation occurs at room temperature in cast alloys with 10% Mg [1]. It has been studied in various applications [1,2], however, research has emerged suggesting its application as an energetic material through corrosive processes [3,4]. Aluminum reacts rapidly with atmospheric oxygen forming a thin layer of aluminum oxide (Al2O3) on its surface. The Al2O3 layer prevents oxygen from coming into contact with the metal, providing protection from corrosion deterioration, making it a metallic material with remarkable corrosion resistance. In recent research [5,6], the behavior of intergranular corrosion in aluminum alloys forming galvanic microcells in saline aqueous media has been studied. Aluminum due to its equivalent weight is an excellent hydrogen producer, due to its negative redox potential [22,24], aluminum reacts easily with water, producing gaseous hydrogen according to equation (1) [7,8] and Al $(OH)_3$.

$$2Al + 3H_2O \rightarrow 3H_2 + Al_2O_3 \quad (1)$$

In equation (1), two moles of Al are observed reacting with three moles of H_2 O, producing 3 moles of H_2 and 〖Al〗_2 O_3. However, the reactions of aluminum with NaOH in aqueous media produce 3H_2, in the following equations [7,8]:

$$2Al + 6H_2O + 2NaOH \rightarrow 2Al(OH)_4 + 3H_2 \quad (2)$$

$$NaAl(OH)_4 \rightarrow NaOH + Al(OH)_3 \quad (3)$$

$$2Al(OH_3) \rightarrow Al_2O_3 + 3H_2 \quad (4)$$

In equation (2) and (3), it is observed that 2 moles of Al react with 6 moles of H2O and 2 moles of NaOH, resulting in 2 moles of Al(〖OH)〗_4 and NaAl(O〖H)〗_4 and 3 moles of H_2. Equation (3) shows the decomposition of (NaAl(OH)_4) into NaOH and Al(〖OH)〗_3 to produce one mole of 〖Al〗_2 O_3 and 3 moles of H_2 O (see Equation (4)). The H_2 produced through these reactions in aqueous solution can be used in mechanical elements, electronic devices, batteries, fuel cells, among others.

2.- Experimental Methodology

2.1.- Materials and heat treatment

For this research, commercial aluminum Al-6063 and magnesium at 99.99% purity were used. The stoichiometric ratio for 2 kg of castings to obtain the alloy (Al80Mg20% weight) is shown in Table 1.

Table 1 Stoichiometric ratio to obtain the alloy Al80Mg20%wt

Aluminum (Al)	1632.38 g
Magnesium (Mg)	367.6 g

Source: Own Elaboration

The melting was performed in a PREFINSA model HR C4/1200 electric resistance furnace (see Figure 1a), at a temperature of 715°C. A graphite crucible was introduced into the furnace to obtain a homogeneous temperature. Then, pieces of Al and Mg were added inside the crucible for melting, placing first the one with the highest melting point and then the one with the lowest melting point. After controlling the melting and the total homogeneity of the casting, the molten metals were poured into a commercial steel mold with rectangular geometry and shape, then the casting was left to cool for 12 hours at room temperature, after which the mold was demolded to obtain the Al80Mg20% wt.% alloy (see Figure 1b).

Figure 1 PREFINSA electric furnace b) Specimens (Al80Mg20% weight))

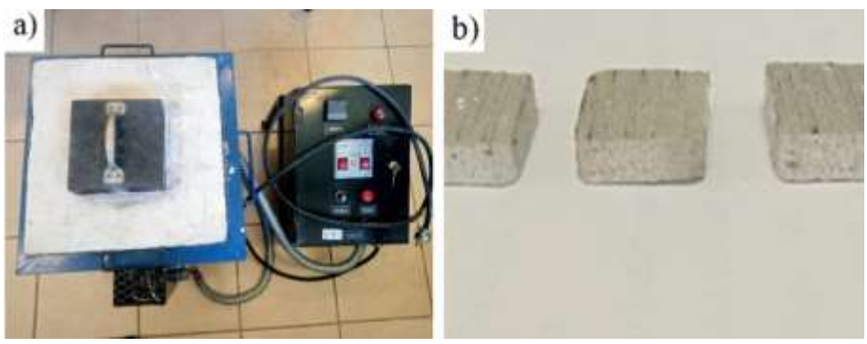

Source: Own Elaboration

To determine the influence of the microstructure and the phases present in Al80Mg20 wt.%, a heat treatment was designed consisting of a solubilization at 300°C (Al80Mg20-24TT) and 350°C (Al80Mg20- 6TT), for 24 and 6 hours, respectively. In both metallurgical situations, they were quenched in ice water at -3°C [9]. Finally, all the specimens were subjected to aging for 6 hours at179°C, allowing them to cool to room temperature, in order to promote the growth of intermetallic phases in this alloy. Figure 1.1 shows the heat treatment diagram used.

Figure 1.1 Heat treatment design

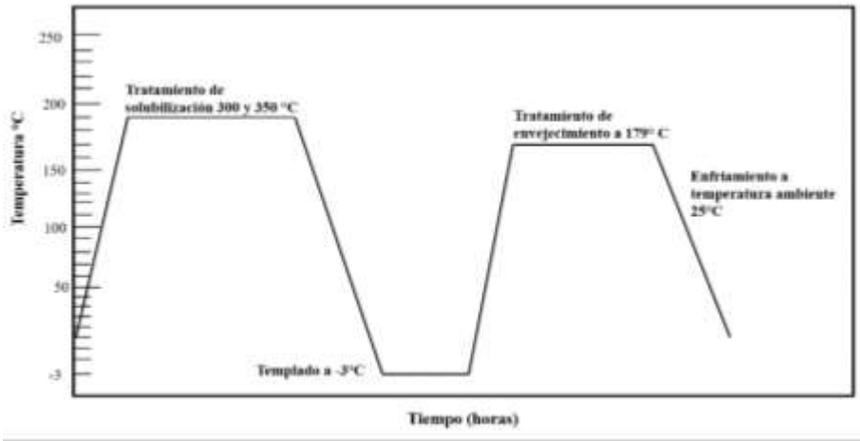

Source: Own Elaboration

2.2. Microstructural characterization of Al80Mg20, Al80Mg20-24TT300 and Al80Mg20-6TT350 alloys

For microstructural characterization, 10 mm x 10 mm x 10 mm specimens were cut from Al80Mg20, Al80Mg20-24TT300°C and Al80Mg20-6TT350°C alloys and roughened with SiC sandpaper from 180 to 2500 grit size. They were then polished to a mirror finish using 1/10µm, 1/2µm and 3µm diamond paste according to ASTM E3-11 [10]. The specimens were dried with distilled water and hot air. Finally, the specimens were chemically attacked with Keller solution (2 ml HF, 3 ml HCl, 5 ml HNO3, 190 ml H2O). The microstructural characterization of the Al80Mg20, Al80Mg20, 24TT300 and Al80Mg20-6TT350 alloy was carried out using an optical microscope (OM), ZEISS Omax-01 brand and a scanning electron microscope (SEM), JEOL-JSM brand. The phases present in the study specimens were identified using an ADP 2000 diffractometer, with Cu-Kα radiation and a wavelength (λ) =1.5406 Å and voltage of 35kV and a current emission of 30mA. The data were collected over a 2θ range from 20° to 80° with a step of 0. 0166.

2.2. Electrochemical tests

Specimens of 1.2 cm x 1.2 cm x 1 cm of Al80Mg20, Al80Mg20, Al80Mg20-24TT300°C and Al80Mg20-6TT350°C alloys were cut and surface prepared. Surface roughing of one side of the samples consisted of sanding with silicon carbide (CSi), with grit sizes from 100 to 600, achieving an effective working surface of 1 cm2. Synthetic seawater at pH: 8.2 [11], a conventional three-electrode cell consisting of: a calomelane reference electrode (ERC), a graphite rod as auxiliary electrode (EA) and Al80Mg20, Al80Mg20-24TT300°C and Al80Mg20-6TT350°C alloy specimens, as working electrode (ET), were used. With the intention of evaluating the influence of the thermal treatment on the specimens and to know the possibility of being used as an energetic material for the generation of (H2), electrochemical tests consisting of potentiodynamic polarization curves (CPP) [12] and resistance to polarization (Rp) [13] were practiced. The CPPs were performed over a range of -1000 mV to -2000 mV with respect to the open circuit potential (OCP) at a sweep speed of 1 mV/s. Corrosion current density was calculated by Tafel extrapolation, considering a range of ±120 mV. All tests were performed at room temperature on an ACM Instruments potentiostat/galvanostat.

3. Results

3.1 Microstructural characterization of Al80Mg20, Al80Mg20-24TT300 and Al80Mg20-6TT350 alloys

Figure 1.2, shows the morphological evolution in cast (Al80Mg20%wt) and heat-treated (Al80Mg20-24TT300°C and Al80Mg20-6TT350°C) condition. The MO shown in Figure 1.2a, revealed the presence of an α Al phase (Mg solid solution) with a globular morphology, surrounded by an intermetallic β secondary phase (Al3Mg2), both with an FCC crystalline structure [14,15,16]. After solubilization heat treatment at 300°C for 6 hours, the micrograph (Figure 1.2b) revealed precipitated particles in the form of elongated globules. However, after 350°C for 24 hours in (Figure 1.2c), precipitation is observed in the form of thick elongated lines, white areas where precipitation is delayed and black areas where it is accelerated [17,18]. Hamana et.al (2018), indicated that the precipitation is the β-phase (Al3Mg2), which originates due to the increase in temperature between ranges of 50°C to 350°C. The morphology obtained in the microstructures has been previously related to similar transformations at various Mg weight contents [18], with longer aging times. The phases studied are clearly identified in the Al-Mg phase diagram [19] and related to the results obtained in X-ray diffraction, (Figure 1.3).

Figure 1.2 Alloy morphological evolution a) Al80Mg20 b) Al80Mg20-6TT350 and c) Al80Mg20-24TT300 heat-treated Al80Mg20-24TT300

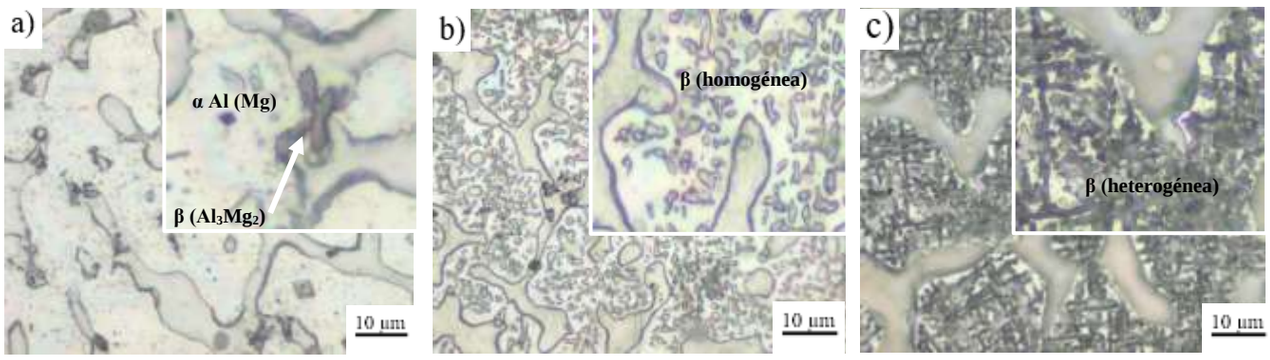

Source: Own Elaboration

Figure 1.3, shows the X-ray diffractograms of Al80Mg20, Al80Mg20-24TT300°C and Al80Mg20-6TT350°C alloys. Two main phases were identified: the Al (Mg) solid solution and the precipitation of the β(Al3Mg2).

Figure 1.3 X-ray diffraction a) Al80Mg20 b) Al80Mg20-6TT350°C and c) Al80Mg20-24TT300°C

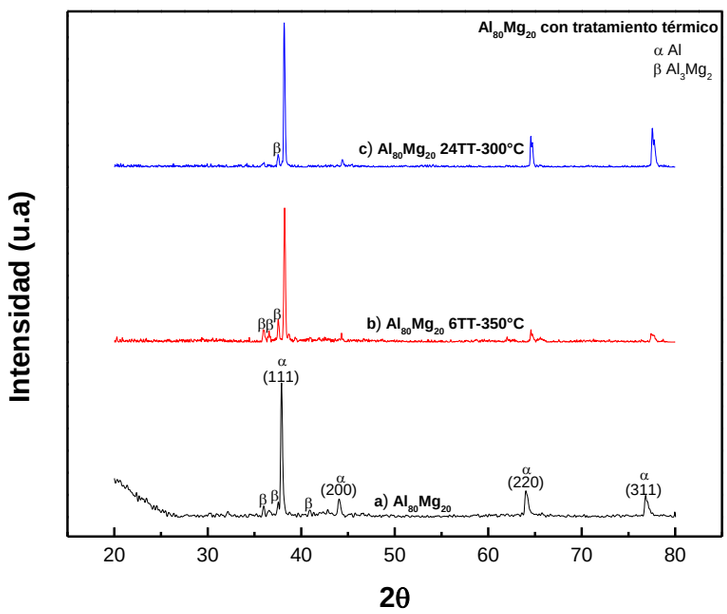

Source: Own Elaboration

In Figure 1.4a, the SEM image of the microstructure corresponding to the Al80Mg20 alloy is observed. The microstructure is composed of an Al matrix (Mg in solid solution) and a secondary intermetallic β-phase (Al3Mg2). Corrosion products were observed in each of the samples, although well differentiated between the different metallurgical conditions, these in general are caused by electrochemical attack. Areas with grain boundary cracking were also identified, this could be due to the redistribution and growth of β (Al3Mg2), which occurs preferentially at the grain boundaries.

The presence of cracking is of interest because it has been reported [5], that this phenomenon is caused by hydrogen embrittlement (H2), referring to equation (1) [7,8]. However, in the (Figure 1.4b, 1.4c), Al80Mg20-6TT350°C and 24TT300°C alloys, the presence of cracking increases at the grain boundaries due to the dissolution of the Al2O3 surface layer under the influence of the intermetallic β(Al3Mg2) phase and solution chemistry, thus causing an acceleration in intergranular corrosion [20,25,26]. In the literature Abdullah *et al*. (2018), indicated that as the NaOH solution increases, the oxide layer on the surface of Al (Mg in solid solution) dissolves faster [7] and that, in turn, more Al contact area can be accessed to react with NaOH and increase the corrosive process.

Figure 1.4 Scanning electron microscopy a) Al80Mg20 b) Al80Mg20-6TT350°C and c) Al80Mg20-24TT300°C.

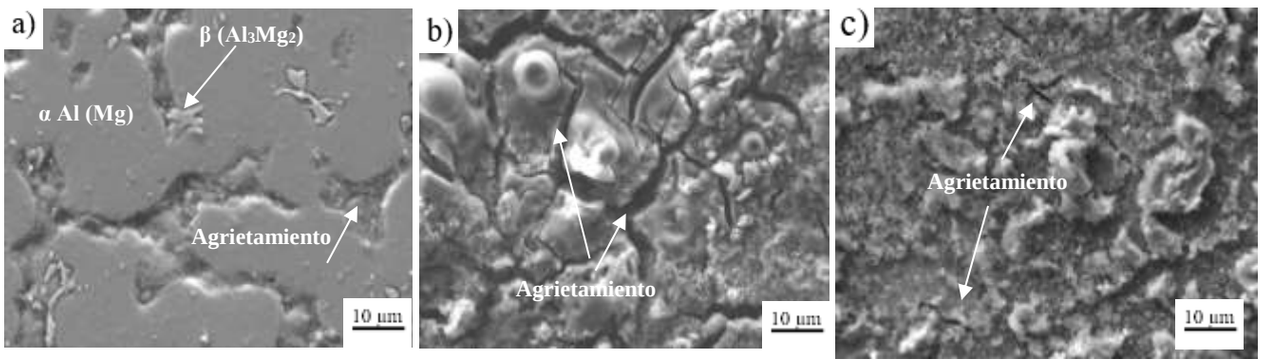

Source: Own Elaboration

3.2. Electrochemical behavior of Al80Mg20, Al80Mg20-24TT300 and Al80Mg20-6TT350 alloys

Figure 1.4 shows the CPP of the alloys Al80Mg20, Al80Mg20-24TT300 and Al80Mg20-6TT350 in synthetic seawater at pH 8.2. The interest in studying the corrosion of this alloy in saline solution, as a hydrogen generator it is known that aluminum produces 2.9 mol H2/m2 per year [5], compared to steels that produce 50% less, so aluminum-based alloys have an interesting energetic potential. Furthermore, in the tests performed in this research it was observed that the microstructure plays an important role in the passivation of the material because the pH was the same for each sample.

The potentiodynamic curves showed that the current density (icorr), increased significantly due to pitting corrosion in point areas, in values ranging from 2.03 mA/cm2 to 3.77 mA/cm2 respectively. However, the potential values did not show significant changes staying around between -1150 mV and -1260mV, indicating that passive films were formed in this potential range [23]. The kinetic parameters obtained from the intersection method are shown in Table 1.2. The icorr was calculated from the Stern-Geary formula at low field, applying a range of ±20 mV. Rp kinetics showed values between 244 Ω*cm2 and 400Ω*cm2. The potentiodynamic results showed a charge transfer controlled behavior, with a slight tendency to form a passive Al2O3 layer as shown in Figure 1.4.

Similarly, the alloy with the presence of the α phase Al (Mg solid solution), acts as a cathode while the β phase (Al3Mg2), acts as an anode, these phases promote the formation of a micro galvanic cell. It can be deduced that the most favorable condition for hydrogen (H2) generation, is the Al80Mg20-24TT300 alloy, with more active Ecorr values [5,21].

Table 1.2 Kinetic parameters obtained from the potentiodynamic polarization curves of the alloy in its different metallurgical conditions: Al80Mg20, Al80Mg20-24TT300°C and Al80Mg20-6TT350°C

Sample	E_{corr} (mV)	I_{corr} (mA)	Ba (mV década)	Bc (mV década)	Rp (Ω*cm^2)
$Al_{80}Mg_{20}$	-1222.18	2.03	-46.91	59.58	400
$Al_{80}Mg_{20}$-6TT350°C	-1153.89	2.57	-18.02	20.56	285.71
$Al_{80}Mg_{20}$-24TT300°C	-1263.72	3.77	-60.45	97.81	244.82

Source: Own Elaboration

Figure 1.4 Potentiodynamic polarization curves Al80Mg20 b) Al80Mg20-6TT350°C and c) Al80Mg20-24TT300°C

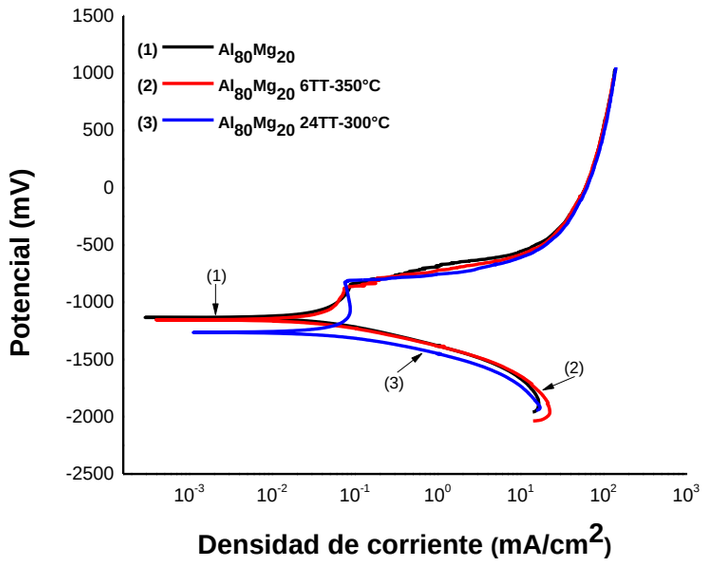

Source: Own Elaboration

Conclusions

The following conclusions can be drawn from this research study:

1. Two main phases were observed from the X-ray diffraction spectra, the Al(Mg solid solution) phase and the secondary interdendritic intermetallic β-phase (Al3Mg2).

2. The microstructure of the material showed changes due to the effects of the thermal treatment of solubilization at 300°C and 350°C for 24 and 6 hours in which precipitates of the β phase (Al3Mg2) were observed in the form of thick and elongated lines due to the nucleation in dispersed zones.

3. The microstructure of the Al80Mg20 base material showed a polygonal type granular behavior corresponding to AlMg alloys.

4. The Al80Mg20-6TT350°C and 24TT300°C showed qualities necessary for the evolution of hydrogen by embrittlement due to the effects of more active potentials; however, the 24TT300°C sample is where the corrosion rate was more accentuated.

Acknowledgments

The author and co-authors would like to thank the Universidad Autónoma del Carmen (UNACAR) and the Instituto de Investigación en Metalurgia y Materiales (IIMM) of the Universidad Michoacana de San Nicolás de Hidalgo (UMSNH) for the use of their facilities and laboratories to carry out this research.

References

[1] Zhao *et al* (2014). *The role of grain boundary plane orientation in the β phase precipitation of an Al–Mg alloy*. Scripta Materialia, p.p 1-4, https://doi.org/10.1016/j.scriptamat.2014.07.003 .

[2] Yi, G., Cullen, D.A., Littrell, K.C. *et al. Characterization of Al-Mg Alloy Aged at Low Temperatures*. Metall Mater Trans A 48, Pages 2-3. https://doi.org/10.1007/s11661-017-3992-2

[3] Martínez *et al* (2019). *Hydrogen generation by aluminum alloy corrosion in aqueous acid solutions promoted by nanometal*: kinetics study. Renewable Energy. Pages 1-7. https://doi.org/10.1016/j.renene.2019.08.103

[4] Dudoladov *et al* (2016). *Generation of hydrogen by aluminum oxidation in aqueous solutions at low temperatures*. International Journal of Hydrogen Energy, Pages 1-8 https://doi.org/10.1016/j.ijhydene.2015.11.122

[5] JE Flores-Chan, A. Torres-Islas, C. Patiño-Carachure, G. Rosas-Trejo & MA Espinosa-Medina (2021) *Comportamiento de corrosión de aleación intermetálica de Al–20Cu en agua de mar sintética*, Canadian Metallurgical Trimestral, 60:3, Pages 1-5, https://doi.org/10.1080/00084433.2021.1997263

[6] Olivares *et al* (2012). *Hydrogen Generation by Treatment of Aluminium Metal with Aqueous Solutions*: Procedures and Uses. In Tech. https://doi.org10.5772/48762

[7] Irankhah, A., Seyed Fattahi, S. M., & Salem, M. (2018). *Hydrogen generation using activated aluminum/water reaction*. International Journal of Hydrogen Energy. Pages 1-6 https://doi.org/10.1016/j.ijhydene.2018.07.014

[8] Wang *et al* (2011). *Generation of hydrogen from aluminum and water – Effect of metal oxide nanocrystals and water quality*. International Journal of Hydrogen Energy, Pages 1-8. https://doi.org/10.1016/j.ijhydene.2011.08.077

[9] M. Araghchi, H. Mansouri & R. Vafaei (2017). *Influencia del tratamiento térmico criogénico en las propiedades mecánicas de una aleación de Al–Cu–Mg*, Ciencia y tecnología de materiales. Pages 1-5, https://doi.org/10.1080/02670836.2017.1407553

[10] ASTM. *"Standard Guide for Preparation of Metallographic Specimens"*. ASTM E3-11. 2da Edition. Pennsylvania: Ed. ASTM International, 2015. https://www.academia.edu/35989703/ASTM_E_3_01_Standard_Guide_for_Preparation_of_Metallographic_Specimens_1?auto=download&email_work_card=download-paper

[11] Standard, A.S.T.M, D. (1998). 1141-98: "*Standard Practice for the Preparation of Substitute Ocean Water"*. American Society for Testing and Materials, USA. https://tienda.aenor.com/norma-astm-d1141-98e1-003143

[12] ASTM, Designation: G5-94, *"Standard Reference Test Method for Making Potentiostatic and Potentiodynamic Anodic Polarization Measurements",* 1993. https://www.astm.org/g0005-94r11e01.html

[13] ASTM, Designation G59-91, "*Standard practice for conducting Potentiodynamic Polarization Resistance Measurements"* 2004. https://pdfcoffee.com/astm-g59-pdf-free.html

[14] Holroyd, N.J.H., Scamans, G.M. (2013) *Stress Corrosion Cracking in Al-Zn-Mg-Cu Aluminum Alloys in Saline Environments*. Metall Mater Trans A 44, Pages 1-8 https://doi.org/10.1007/s11661-012-1528-3

[15] George F. V. V. *Metallography and Microstructures*, Volume 9. ASM International. 2004. USA.

[16] KUMAR, S., NAMBOODHIRI, T.K.G. (2016). *Precipitation hardening and hydrogen embrittlement of aluminum alloy AA7020*. Bull Mater Sci 34, Pages 2-5.https://doi.org/10.1007/s12034-011-0066-8

[17] Yang, Y.-K., & Allen, T. (2013). *Direct visualization of β phase causing intergranular forms of corrosion in Al–Mg alloys*. Materials Characterization, 80, Pages 1-4. https://doi.org/10.1016/j.matchar.2013.03.014

[18] Hamana, D., Baziz, L., & Bouchear, M. (2004). *Kinetics and mechanism of formation and transformation of metastable β′-phase in Al–Mg alloys*. Materials Chemistry and Physics, 84(1), Pages 1-6, https://doi.org10.1016/j.matchemphys.2003.11.001

[19] T.B Massalki, H Okamoto, P.R. Subramanian, L. Kacprzak, W.W. Scott, *Binary Alloy Phase Diagrams, ASMT International*, Vol 1, (1986), Metals Park, OH: American society for metals.

[20] Grimm *et al* (2019), *Influence of the microstructure on the corrosion behaviour of cast Mg-Al alloys*, Corrosion Science, Volume 155, Pages 1-3, ISSN 0010-938X, https://doi.org/10.1016/j.corsci.2019.04.024

[21] Liu *et al* (2017). *Pitting Corrosion of Steel Induced by Al_2O_3 Inclusions*. Metals, 7(9), Pages 1-8 https://doi.org/10.3390/met7090347

[22] Mendoza Márquez, O.J. (2020) *Evaluación del Mecanismo de Corrosión del Aluminio y sus Aleaciones Al-5154 y Al-6063 para la producción de Hidrógeno*. [Tesis de Maestría]. Universidad Autónoma del Carmen.

[23] Zhang *et al* (2020). *Influence of heat treatment on corrosion behavior of rare earth element Sc modified Al-Mg alloy processed by selective laser melting*. Applied Surface Science, https://doi.org/10.1016/j.apsusc.2020.145330

[24] Flores Chan J.E. (2018). *Evaluación de la corrosión en intermetálicos Al-Me20% peso (Me=Fe, Cu y Mg) en agua de mar sintética, empleando técnicas electroquímicas CP, RPL y EIE* [Disertación Doctoral, Universidad Michoacana de San Nicolas de Hidalgo]. Repositorio de la UMSNH. http://bibliotecavirtual.dgb.umich.mx:8083/xmlui/handle/DGB_UMICH/1321

[25] Zhang *et al* (2020*). Current-driving intergranular corrosion performance regeneration below the precipitate's solvus temperature in Al–Mg alloy*. Journal of Materials Science & Technology, 53, Pages 1-5. https://doi.org/10.1016/j.jmst.2020.01.071

[26] Yi *et al* (2017). *Characterization of Al-Mg Alloy Aged at Low Temperatures*. Metallurgical and Materials Transactions A, 48(4), Pages 1-9. https://DOI.org10.1007/s11661-017-3992-2